ACCSCIENCE PUBLISHING

Green Technology & Innovation

ARTICLE

Energy and exergy analysis of the XYZ ultra-supercritical steam power plant

Fadhlin Nurul Izzah*, Berkah Fajar Tamtomo Kiono*, and Khoiri Rozi

Department of Mechanical Engineering, Faculty of Engineering, Diponegoro University, Semarang, Central Java, Indonesia

Abstract

The increasing electricity demand, propelled by economic expansion and population growth, underscores the critical need for dependable power generation. Steam power plants (SPPs) remain a cornerstone of Indonesia's electricity production, particularly those fuelled by coal. Energy conservation in SPPs is paramount, focusing on enhancing energy efficiency. However, the current performance assessment, solely based on energy efficiency, overlooks crucial aspects of energy utilization, necessitating a combined approach integrating exergy analysis. This study aims to identify the energy and exergy efficiencies in ultra-supercritical (USC) SPPs, providing management guidelines to prioritize improvement efforts for enhancing thermodynamic efficiency in the XYZ USC SPP system. Previous research has highlighted significant exergy destruction in boilers and turbines. Hence, this study aimed to evaluate the energy and exergy analyses at 100%, 75%, and 50% loads on the XYZ USC SPPs unit. The Engineering Equation Solver software was used for the analysis. The power plant efficiencies were 46.94%, 47.01%, and 47.03% at 50%, 75%, and 100% loads. The largest exergy destruction occurred in the boiler, with 1,918 MW at 50% load, 1,609 MW at 75% load, and 1,416 MW at 100% load. The smallest exergy destruction occurred in the condensate extraction pump, with 1.441 MW at 50% load, 1.457 MW at 75% load, and 1.544 MW at 100% load. These findings from the XYZ USC SPP demonstrate that, although the plant achieves competitive energy efficiency levels, substantial opportunities remain for thermodynamic enhancement. The exergy analysis identifies the boiler as the principal source of exergy loss, largely due to inefficiencies in combustion and heat transfer processes. In addition, turbines – particularly the low-pressure turbine – also contribute to significant exergy destruction, warranting targeted optimization efforts.

Keywords: Energy; Exergy destruction; Efficiency; Steam power plants; Engineering equation solver

***Corresponding authors:**
Fadhlin Nurul Izzah (fadhlinnurulizzah@students.undip.ac.id)
Berkah Fajar Tamtomo Kiono (fajarberkah10@lecturer.undip.ac.id)

Citation: Izzah FN, Kiono BFT, Rozi K. Energy and exergy analysis of the XYZ ultra-supercritical steam power plant. *Green Technol Innov*. 2025;1(1):8099. doi: 10.36922/gti.8099

Received: December 20, 2024

Revised: March 28, 2025

Accepted: April 7, 2025

Published online: April 25, 2025

1. Introduction

Electric demand rises annually due to population and economic growth, societal welfare improvements, and technological advancements.[1] Reliable power plants are crucial to meet this increasing demand. In Indonesia, steam power plants (SPPs), primarily coal-based, play a key role in electricity generation. The Electricity Supply Business Plan 2021 – 2030 predicts coal will remain dominant until 2030, accounting for 59.4% of

the energy sector. Coal-fired power generation is expected to increase from 194, 558 GWh in 2021 to 264, 260 GWh in 2030.[2] SPPs convert thermal energy from steam into electrical energy using boilers, turbines, generators, condensers, pumps, and heaters.

In this context, the ultra-supercritical (USC) SPP technology emerges as a promising solution. USC technology operates at higher pressures and temperatures than conventional coal-fired power plants, enabling improved thermal efficiency and reduced carbon emissions.[3] Eguchi *et al.*,[4] Zhang and Wang,[5] Nikam *et al.*,[6] and Rocha *et al.*[7] state that the thermal efficiency of USC power plants can reach up to 50%, significantly reducing fuel consumption and carbon dioxide (CO_2) emissions. However, despite the considerable potential of USC technology, it is essential to conduct a comprehensive energy and exergy performance analysis of the system to identify opportunities for further optimization.

Currently, power plant performance is assessed primarily based on energy efficiency, grounded in the first law of thermodynamics. However, this approach does not adequately reflect critical aspects of energy utilization, as it only measures the quantity of energy consumed without considering its quality.[8] Therefore, an exergy-based approach, grounded in the second law of thermodynamics, is necessary to understand a power plant's efficiency better. Energy assessments should consider both quantity and quality. In recent decades, exergy analysis, based on the second law, has emerged as a practical approach for designing, evaluating, optimizing, and improving coal-fired power plants. Exergy analysis allows for a comprehensive evaluation of each component's performance and contribution to system irreversibility, enabling precise identification of energy losses.[9] Therefore, assessing energy and exergy efficiency is critical for comprehensively understanding power plant performance. Combining energy and exergy efficiency analysis provides deeper insights into the performance of various machine components.

Several researchers have assessed energy and exergy in various power plants. Studies by Han *et al.*[10] and Chen *et al.*[11] showed that energy and exergy analyses reveal performance declines and significant losses due to exergy destruction, causing inefficiencies in power plants. Khaleel *et al.*[12] compared energy and exergy analyses of coal and gas-fired thermal power plants, highlighting that combustion chambers significantly contribute to exergy destruction due to their irreversible nature. Their findings showed an exergy efficiency of around 20% for the entire system, with significant losses in the boiler and steam turbine. Adibhatla and Kaushik[13] analyzed the energy and exergy of a 660 MW supercritical power plant in India and noted substantial exergy destruction in the boiler and turbine. They found that sliding pressure operation can reduce exergy destruction, especially under partial load conditions. Pambudi *et al.*[14] performed exergy analysis and optimization of a geothermal power plant using Engineering Equation Solver (EES) software based on thermodynamic laws. The analysis results show that the exergy of the discharged geothermal fluid generates 21.71 MW of electricity with a second-law efficiency of 36.48%. Optimization was performed by reducing the separator pressure, resulting in a power increase of 20 kW. Kaushik *et al.*[15] detailed methodologies for energy and exergy analyses of thermal power plant components and concluded that the most significant exergy losses occur in the boiler. Kumar *et al.*[16] investigated coal-fired thermal power plants, emphasizing a 210 MW unit, finding substantial energy losses in the condenser (64.24%) and significant exergy destruction in the boiler (88.91%). Abuelnuor *et al.*[17] focused on energy and exergy aspects in Khartoum North Power Plant, identifying the chimney as a significant energy disposal source (18% of total energy input) and the combustion chamber as a substantial energy loss contributor (39.8%). Khaleel *et al.*[18] modeled and analyzed the optimal performance of coal-fired power plants based on energy evaluation, examining the effects of steam extraction pressure and feedwater heater configuration on plant performance. They determined the optimal steam extraction pressure for feedwater heaters to maximize energy and exergy efficiency. They found that increased deaeration pressure improves thermal and exergy efficiency, albeit with decreased net power generation.

Building on this research, this study provides a comprehensive energy and exergy analysis of the 1,070 MW XYZ USC SPP. The novelty of this work lies in its detailed investigation of this specific plant, including a component-level analysis of exergy destruction and efficiency across three different load conditions (100%, 75%, and 50% of normal continuous rating). A model was developed using the EES software to perform these energy and exergy analyses. By identifying the components with the highest exergy destruction and analyzing the efficiency trends, this study provides specific recommendations for optimizing the plant's thermodynamic performance.

2. Data and methods

2.1. Description of the XYZ SPP

USC power plants offer significant operational advantages, including improved efficiency and adaptability to sliding pressure operations. These capabilities allow them to respond quickly to load changes, reducing startup times and enhancing operational flexibility.[19,20] Integrating

advanced materials and control technologies enables USC plants to handle high temperatures and pressures effectively, ensuring consistent performance under variable operating conditions.[21] This paper focuses on the XYZ SPP, which has a capacity of 1,070 MW. We selected three load conditions: 100% (1,070 MW), 75% (802.5 MW), and 50% (535 MW) of the plant's normal continuous rating.

The continuous mass flow diagram for a USC, as described in this study, includes key components such as the high-pressure turbine (HPT), intermediate-pressure turbine (IPT), low-pressure turbine (LPT), boiler (B), condensate extraction pump (CEP), boiler feed pump (BFP), low-pressure heater (LPH), high-pressure heater (HPH), deaerator (D), and generator, as depicted in Figure 1. The boiler in this power plant produces superheated steam at a pressure of 250 bar (250×10^5 Pa) and a temperature of 600°C (873.15 K) at the superheater outlet, with a steam flow rate of 806.86138889 kg/s. The system features a single reheating stage at 600°C (873.15 K). The cold reheat steam is reheated to prevent high moisture content in the final stages of the LPT. Steam extraction from the last stage of the HPT is utilized for feedwater regeneration in the final HPH.

2.2. Work parameters data

Work parameters data used for the energetic and exergetic analysis of the XYZ supercritical SPP are obtained from testing and the heat balance diagram of the plant. The temperature-entropy diagram is shown in Figure 2, and the operational data can be seen in Table 1.

The results of the coal analysis are shown in Table 2. The higher heating value is 4,541.88 kcal/kg (18,991 kJ/kg).

The specific heat, mass flow, and temperature of the flue gas and air supply to the boiler are tabulated in Table 3.

2.3. Energetic calculation equations

In an open flow system, energy transfer across the control volume can occur in three forms: Work transfer, heat transfer, and energy associated with mass transfer. This relationship is mathematically expressed by applying the first law of thermodynamics to a steady-flow process in an open system, as follows in Equation I,

$$\dot{Q}_{cv} + \sum_i \dot{m}_i \left(h_i + \frac{V_i^2}{2} + gz_i\right) = \dot{W}_{cv} + \sum_e \dot{m}_e \left(h_e + \frac{V_e^2}{2} + gz_e\right) \quad \text{(I)}$$

Where $\dot{Q}_{cv}$ is heat transfer rate (kW), $\dot{W}_{cv}$ is work (kW), $\dot{m}$ is the mass flow rate (kg/s), is enthalpy (kJ/kg), V = velocity (m/s), g is acceleration of gravity (m/s^2), and z is elevation (m). The subscript "i" indicates the state of the inlet fluid, and "e" indicates the state of the exiting destruction rate of fluid (kW).

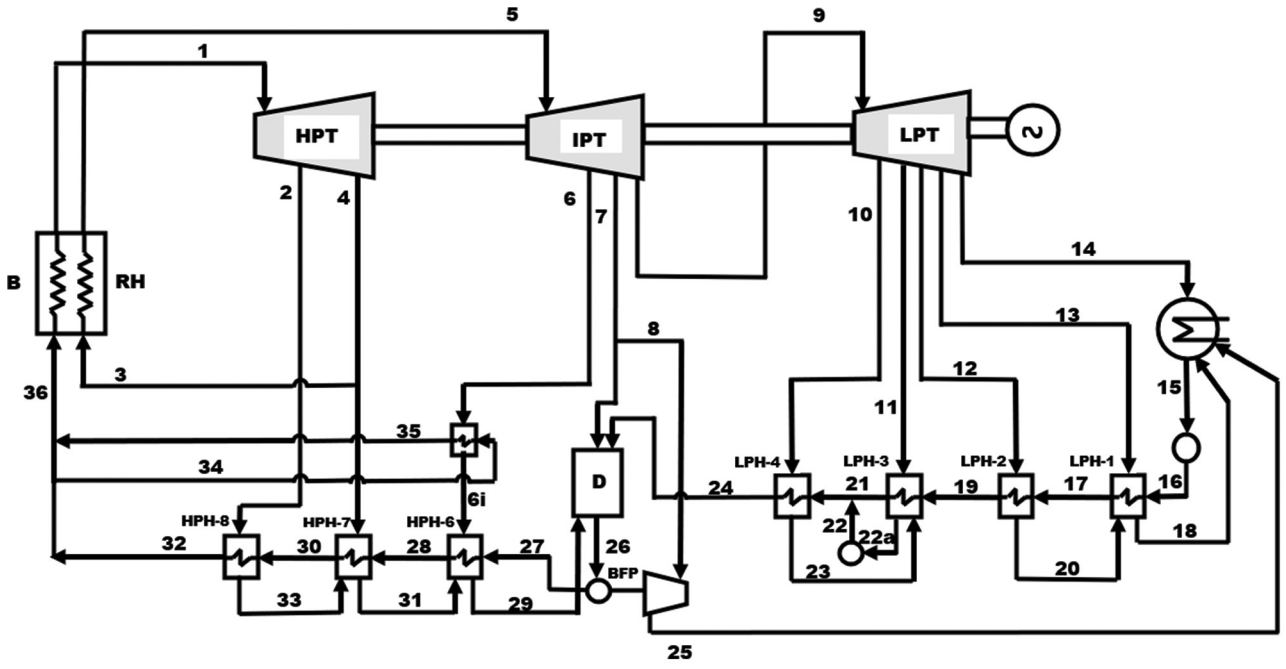

Figure 1. Simplified schematic view of 1,070 MW XYZ supercritical steam power plant
Abbreviations: BFP: Boiler feed pump; CEP: Condensate extraction pump; D: Deaerator; HPH: High-pressure heater; HPT: High-pressure turbine; IPT: Intermediate-pressure turbine; LPH: Low-pressure heater; LPT: Low-pressure turbine.

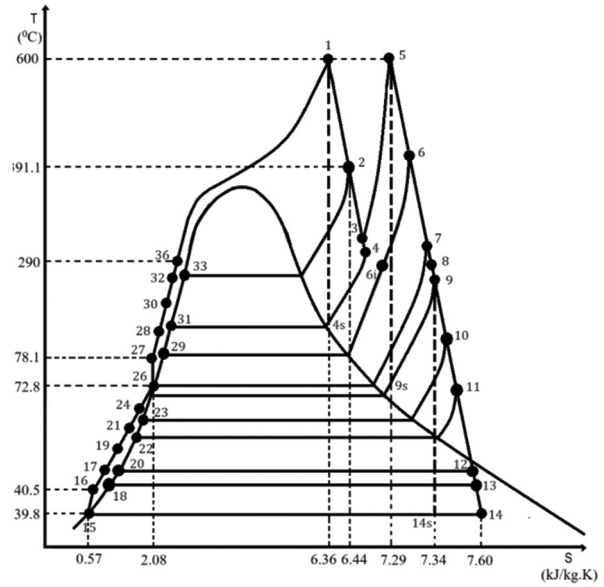

Figure 2. The temperature-entropy diagram of the process

The energy balance for the boiler is given in Equation II,

$$0 = \dot{Q}_b - \dot{m}_1\left(h_1 - h_{36}\right) - \dot{m}_5\left(h_5 - h_4\right) \quad \text{(II)}$$

Where $\dot{m}_1$ is the mass flow rate of feedwater entering the boiler, $\dot{m}_5$ is the mass flow rate of steam entering the reheater, and $\dot{Q}_b$ the rate of heat transfer to the boiler.

The energy balance for the HPT is given in Equation III.

$$\dot{W}_{HPT} = \dot{m}_1\left(h_1 - h_2\right) + (\dot{m}_1 - \dot{m}_2)\left(h_2 - h_3\right) \quad \text{(III)}$$

The energy balance for the IPT is given in Equation IV.

$$\begin{aligned}\dot{W}_{IPT} &= \dot{m}_5\left(h_5 - h_6\right) + \left(\dot{m}_5 - \dot{m}_6\right)\left(h_6 - h_7\right) \\ &+ \left(\dot{m}_5 - \dot{m}_6 - \dot{m}_7\right)\left(h_7 - h_8\right) + (\dot{m}_5 - \dot{m}_6 - \dot{m}_7 - \dot{m}_8)\left(h_8 - h_9\right)\end{aligned} \quad \text{(IV)}$$

The energy balance for the LPT is given in Equation V.

$$\begin{aligned}\dot{W}_{LPT} &= \dot{m}_9\left(h_9 - h_{10}\right) + \left(\dot{m}_9 - \dot{m}_{10}\right)\left(h_{10} - h_{11}\right) \\ &+ \left(\dot{m}_9 - \dot{m}_{10} - \dot{m}_{11}\right)\left(h_{11} - h_{12}\right) \\ &+ (\dot{m}_9 - \dot{m}_{10} - \dot{m}_{11} - \dot{m}_{12})\left(h_{12} - h_{13}\right) \\ &+ (\dot{m}_9 - \dot{m}_{10} - \dot{m}_{11} - \dot{m}_{12} - \dot{m}_{13})\left(h_{13} - h_{14}\right)\end{aligned} \quad \text{(V)}$$

The energy balance for the condenser is given in Equation VI.

$$\dot{m}_{14}h_{14} - \dot{Q}_{cond} = \dot{m}_{15}h_{15} \quad \text{(VI)}$$

The energy balance for the CEP is given in Equation VII.

$$0 = \dot{m}_{16}\left(h_{15} - h_{16}\right) + \dot{W}_{CEP} \quad \text{(VII)}$$

The energy balance for the BFP is given in Equation VIII.

$$0 = \dot{m}_{27}\left(h_{26} - h_{27}\right) + \dot{W}_{BFP} \quad \text{(VIII)}$$

The energy balance for the LPH-1 is given in Equation IX.

$$0 = \dot{m}_{13}\left(h_{13} - h_{17}\right) - \dot{m}_{16}\left(h_{17} - h_{16}\right) \quad \text{(IX)}$$

The energy balance for the deaerator is given in Equation X.

$$0 = \dot{m}_7 h_7 + \dot{m}_{24}h_{24} + \dot{m}_{29}h_{29} - \dot{m}_{26}h_{26} \quad \text{(X)}$$

The energy balance for the HPH-8 is given in Equation XII.

$$0 = \dot{m}_2\left(h_2 - h_{33}\right) - \dot{m}_{30}\left(h_{32} - h_{30}\right) \quad \text{(XI)}$$

2.4. Exergetic calculation equations

The exergy calculation at each point can be analyzed based on the fluid type at that specific point. An open system, or control volume, is a system where mass can flow across boundaries. The equation for the balance of exergy in a control volume and the steady state is as follows in Equation XII,

$$0 = \sum_j (1 - \frac{T_0}{T_j})\dot{Q}_j - \dot{W}_{cv} + \sum_i \dot{m}_i e_{fi} - \sum_e \dot{m}_e e_{fe} - \dot{E}_d \quad \text{(XII)}$$

where $\dot{Q}_j$ is the rate of energy transfer (kW), T_0 is the dead state (K), T_j is the temperature at the system boundary (K), and $\dot{E}_d$ is the exergy destruction rate (kW).

e_{fi} accounts for the exergy per unit of mass entering the inlet *i*, and e_{fe} accounts for the exergy per unit of mass exiting at exit *e*. These terms, known as the specific flow exergy, are expressed as Equation XIII,

$$e_f = h - h_0 - T_0\,(s - s_0) \quad \text{(XIII)}$$

Where e_f is the specific flow exergy (kJ/s or kW), and *s* is entropy (kJ/kg–K).

In Equation XIV, the rate of exergy destruction of exergy due to irreversibilities within the system is symbolized by $\dot{E}_d$. That is,

$$\dot{E}_d = T_0\dot{\sigma} \quad \text{(XIV)}$$

where is $\dot{\sigma}$ the rate of entropy production (kJ/K)

The exergy balance for the boiler is given in Equation XV,

$$0 = \sum\nolimits_c \dot{m}_c e_{fc} - \sum\nolimits_p \dot{m}_p e_{fp} - T_0\dot{\sigma} \quad \text{(XV)}$$

Table 1. Flow stream data of XYZ ultra-supercritical steam power plant at different loads

Stream ID	Mass flow rate (kg/s)			Temperature (°C)			Pressure (×10^5 Pa)		
	100%	75%	50%	100%	75%	50%	100%	75%	50%
1	806.9	590.7	384.6	600	600	600	250	207	137.4
2	46.1	28.24	16.02	391.1	391.9	391.9	67.1	50.5	33.9
3	81.61	52.08	28.06	345.4	345.6	345.6	48.8	36.8	33.9
4	679.2	509.4	340.5	346.7	346.1	353.4	50.3	37.7	25.3
5	679.2	509.4	340.5	600	600	600	47.1	35.3	23.6
6	53.95	39.17	23.79	487.5	489	489	22.6	17.1	11.3
6i	53.95	39.17	23.79	317.1	289.3	263.2	22.6	17.1	11.3
7	34.4	15.71	10,3	343.9	348.4	356.8	8.75	6.52	4.56
8	45.03	29.13	12.61	343.7	348.3	356.2	8.22	6.39	4.45
9	545.8	425.4	293.8	342.5	346.3	356.3	0.0731	6.7	4.66
10	32.44	23.33	14.4	244.2	248.3	254.8	3.71	2.87	2.02
11	22.12	16.55	10.34	144.5	148.3	153.7	1.444	1.12	0.785
12	29.86	20.44	9.078	88.3	81.4	82	0.675	0.495	0.346
13	25.27	26.09	9.378	69	63.4	55.8	0.299	0.233	0.164
14	436.1	339	250.6	39.8	38.2	36.9	0.0731	0.0671	0.0625
15	545.8	425.4	293.8	39.8	38.2	36.9	0.07307	0.0671	0.06248
16	590.8	454.5	306.4	40.5	39.1	38.2	14.51	15.03	12.32
17	590.8	454.5	306.4	88.5	61.8	55.1	15.49	15.58	12.32
18	109.7	86.4	9.378	69.02	63.4	55.83	0.299	0.233	0.164
19	590.8	454.5	306.4	85.5	79.5	71.7	13.14	12.84	13.96
20	84.42	60.32	9.378	88.98	81.07	72.41	0.675	0.495	0.346
21	590.8	454.5	306.4	107.6	101.3	92.3	16.82	12.41	12.23
22	590.8	454.5	306.4	107.6	101.3	92.3	16.82	12.41	12.23
22a	54.56	39.88	24.74	110.2	102.8	92.98	1.444	1.12	0.785
23	32.44	23.33	14.4	140.9	132	120.5	3.71	2.87	2.02
24	590.8	454.5	306.4	138.2	130.5	119.8	11.93	12.85	15.3
25	45.03	29.13	12.61	41.2	38.9	37.4	0.0731	0.0671	0.0625
26	806.9	590.7	384.6	172.8	162.1	148.4	8.472	6.52	4.561
27	806.9	590.7	384.6	178.1	166.4	150.9	317.7	245	167.3
28	806.9	590.7	384.6	218.5	205.2	186.8	300.6	249.9	168.5
29	181.7	120.5	67.87	218.6	204.6	185.3	22.6	17.1	11.3
30	806.9	590.7	384.6	262.4	245.9	223.3	284.2	247.6	169.2
31	127.7	81.32	44.08	262.4	245.5	223.3	48.8	36.8	24.7
32	806.9	590.7	384.6	285	267.2	243	324.5	247	152.1
33	46.1	29.24	16.02	283	264.6	240.7	67.1	50.5	33.9
34	806.9	590.7	384.6	285	267.2	243	324.5	247	152.1
35	242.05	177.2	115.4	301.5	286.2	263.4	302.3	244.2	163.2
36	806.9	590.7	384.6	290	273	279.2	299.6	240.5	160.1

Where $\sum_c \dot{m}_c e_{fc}$ is the sum of exergy fuel, air, feedwater, and cold reheater that enters the boiler, while $\sum_p \dot{m}_p e_{fp}$ is the sum of exergy produced by the boiler in the form of main steam, hot reheat, and flue gas.

Table 2. Coal analysis of the steam power plant

Parameters	Percentage of parameters (%)
Carbon	47.06
Hydrogen	3.42
Nitrogen	0.84
Sulfur	0.271
Oxygen	13.44

Table 3. Specific heat and temperature of a flue gas and air supply to the boiler

Parameters	Specific heat (kJ/kg)	Temperature (°C)	Mass flow (kg/s)
Flue gas	1.078	144.56 (417.71 K)	629.48
Air supply	1.045	28 (301.15 K)	629.48

The exergetic efficiency of the boiler is defined in Equation XVI.

$$\varepsilon_{boiler} = 1 - \frac{T_0 \dot{\sigma}}{\sum_c \dot{m}_c e_{fc}} \quad \text{(XVI)}$$

The exergy balance for the HPT is given in Equation XVII,

$$\dot{W}_{HPT} = \dot{m}_1 (e_1 - e_2) + (\dot{m}_1 - \dot{m}_2)(e_2 - e_3) - T_0 \dot{\sigma} \quad \text{(XVII)}$$

and the exergy destruction is given in Equation XVIII,

$$\dot{E}_{d,HPT} = T_0 \dot{\sigma} = T_0 (\dot{m}_1 (s_2 - s_1) + (\dot{m}_1 - \dot{m}_2)(s_3 - s_2)) \quad \text{(XVIII)}$$

Where $\dot{E}_{d,HPT}$ is the rate of exergy destruction in the HPT.

The second law of efficiency for HPT can be expressed as Equation XIX.

$$\varepsilon_{HPT} = 1 - \frac{\dot{E}_{d,HPT}}{\dot{m}_1 (e_1 - e_2) + (\dot{m}_1 - \dot{m}_2)(e_2 - e_3)} \quad \text{(XIX)}$$

The exergy balance for the IPT is given as Equation XX,

$$\begin{aligned} \dot{W}_{IPT} &= \dot{m}_5 (e_5 - e_6) + (\dot{m}_5 - \dot{m}_6)(e_6 - e_7) \\ &+ (\dot{m}_5 - \dot{m}_6 - \dot{m}_7)(e_7 - e_8) \\ &+ (\dot{m}_5 - \dot{m}_6 - \dot{m}_7 - \dot{m}_8)(e_8 - e_9) - T_0 \dot{\sigma} \end{aligned} \quad \text{(XX)}$$

and the exergy destruction is given in Equation XXI,

$$\begin{aligned} \dot{E}_{d,IPT} &= T_0 \dot{\sigma} = T_0 \dot{m}_5 (s_6 - s_7) + (\dot{m}_5 - \dot{m}_6)(s_7 - s_8) \\ &+ (\dot{m}_5 - \dot{m}_6 - \dot{m}_7)(s_8 - s_7) + (\dot{m}_5 - \dot{m}_6 - \dot{m}_7 - \dot{m}_8)(s_9 - s_8)) \end{aligned} \quad \text{(XXI)}$$

where $\dot{E}_{d,IPT}$ is the rate of exergy destruction in the IPT.

The exergetic efficiency for IPT is defined as Equation XXII.

$$\begin{aligned} \varepsilon_{IPT} = 1 - \frac{\dot{E}_{d,IPT}}{} & \\ \dot{m}_5 (e_5 - e_6) + (\dot{m}_5 - \dot{m}_6)(e_6 - e_7) & \\ + (\dot{m}_5 - \dot{m}_6 - \dot{m}_7)(e_7 - e_8) & \\ + (\dot{m}_5 - \dot{m}_6 - \dot{m}_7 - \dot{m}_8)(e_8 - e_9) & \end{aligned} \quad \text{(XXII)}$$

The exergy balance for the LPT is given as Equation XXIII.

$$\begin{aligned} \dot{W}_{LPT} &= \dot{m}_9 (e_9 - e_{10}) + (\dot{m}_9 - \dot{m}_{10})(e_{10} - e_{11}) \\ &+ (\dot{m}_9 - \dot{m}_{10} - \dot{m}_{11})(e_{11} - e_{12}) \\ &+ (\dot{m}_9 - \dot{m}_{10} - \dot{m}_{11} - \dot{m}_{12})(e_{12} - e_{13}) \\ &+ (\dot{m}_9 - \dot{m}_{10} - \dot{m}_{11} - \dot{m}_{12} - \dot{m}_{13})(e_{13} - e_{14}) - T_0 \dot{\sigma} \end{aligned} \quad \text{(XXIII)}$$

where the flow exergy in the LPT is given in Equation XXIV,

$$\begin{aligned} e_{LPT} &= \dot{m}_9 (e_9 - e_{10}) + (\dot{m}_9 - \dot{m}_{10})(e_{10} - e_{11}) \\ &+ (\dot{m}_9 - \dot{m}_{10} - \dot{m}_{11})(e_{11} - e_{12}) \\ &+ (\dot{m}_9 - \dot{m}_{10} - \dot{m}_{11} - \dot{m}_{12})(e_{12} - e_{13}) \\ &+ (\dot{m}_9 - \dot{m}_{10} - \dot{m}_{11} - \dot{m}_{12} - \dot{m}_{13})(e_{13} - e_{14}) - T_0 \end{aligned} \quad \text{(XXIV)}$$

and the exergy destruction is given in Equation XXV.

$$\begin{aligned} \dot{E}_{d,LPT} &= T_0 \dot{\sigma} = T_0 \dot{m}_9 (s_{10} - s_9) + (\dot{m}_9 - \dot{m}_{10})(s_{11} - s_{10}) \\ &+ (\dot{m}_9 - \dot{m}_{10} - \dot{m}_{11})(s_{12} - s_{11}) \\ &+ (\dot{m}_9 - \dot{m}_{10} - \dot{m}_{11} - \dot{m}_{12})(s_{13} - s_{12}) \\ &+ (\dot{m}_9 - \dot{m}_{10} - \dot{m}_{11} - \dot{m}_{12} - \dot{m}_{13})(s_{14} - s_{13})) \end{aligned} \quad \text{(XXV)}$$

The second law of efficiency for LPT can be expressed as Equation XXVI.

$$\varepsilon_{LPT} = 1 - \frac{\dot{E}_{d,LPT}}{e_{LPT}} \quad \text{(XXVI)}$$

The exergy balance for the condenser is given as Equation XXVII.

$$\dot{E}_{d,cond} = \dot{m}_{14} e_{14} - \dot{m}_{15} e_{15} - (1 - \frac{T_0}{T_9}) \dot{Q}_{cond} \quad \text{(XXVII)}$$

The second law of efficiency

$\dot{E}_{d,cond} = \dot{m}_{14} e_{14} - \dot{m}_{15} e_{15} - (1 - \frac{T_0}{T_9}) \dot{Q}_{cond}$ for the condenser is given in Equation XXVIII.

$$\varepsilon_{cond} = 1 - \frac{\dot{E}_{d,cond}}{\dot{m}_{14}e_{14} - \dot{m}_{15}e_{15}} \quad \text{(XXVIII)}$$

The exergy balance for the CEP is given as Equation XXIX.

$$\dot{E}_{d,CEP} = T_0\dot{\sigma} = \dot{m}_{16}\left(e_{15} - e_{16}\right) + \dot{W}_{CEP} = \dot{m}_{16}T_0\left(s_{16} - s_{15}\right) \quad \text{(XXIX)}$$

The second law of efficiency for CEP is:

$$\varepsilon_{CEP} = 1 - \frac{\dot{E}_{d,CEP}}{\dot{W}_{CEP}} \quad \text{(XXX)}$$

The exergy balance for the BFP is given as Equation XXXI.

$$\dot{E}_{d,BFP} = T_0\dot{\sigma} = \dot{m}_{27}\left(e_{26} - e_{27}\right) + \dot{W}_{BFP} = \dot{m}_{27}T_0\left(s_{27} - s_{26}\right) \quad \text{(XXXI)}$$

The second law of efficiency for BFP is given in Equation XXXII.

$$\varepsilon_{BFP} = 1 - \frac{\dot{E}_{d,BFP}}{\dot{W}_{BFP}} \quad \text{(XXXII)}$$

The exergy balance for the deaerator is given as Equation XXXIII.

$$\dot{E}_{d,deaerator} = T_0\dot{\sigma} = \dot{m}_7e_7 + \dot{m}_{24}e_{24} + \dot{m}_{29}e_{29} - \dot{m}_{26}e_{26} \quad \text{(XXXIII)}$$

The second law of efficiency for the deaerator is given in Equation XXXIV.

$$\varepsilon_{deaerator} = 1 - \frac{\dot{E}_{d,deaerator}}{\dot{m}_7e_7 + \dot{m}_{24}e_{24} + \dot{m}_{29}e_{29}} \quad \text{(XXXIV)}$$

The exergy balance for the LPH-1 is given as Equation XXXV.

$$\dot{E}_{d,LPH1} = T_0\dot{\sigma} = \dot{m}_{13}\left(e_{13} - e_{17}\right) - \dot{m}_{16}\left(e_{17} - e_{16}\right) \quad \text{(XXXV)}$$

The second law of efficiency for LPH-1 is given in Equation XXXVI.

$$\varepsilon_{LPH1} = 1 - \frac{\dot{E}_{d,LPH1}}{\dot{m}_{13}\left(e_{13} - e_{17}\right)} \quad \text{(XXXVI)}$$

The exergy balance for the HPH-8 is given as Equation XXXVII.

$$\dot{E}_{d,HPH8} = T_0\dot{\sigma} = \dot{m}_2\left(e_2 - e_{33}\right) - \dot{m}_{30}\left(e_{32} - e_{30}\right) \quad \text{(XXXVII)}$$

The second law of efficiency for HPH-8 is given in Equation XXXVIII.

$$\varepsilon_{HPH8} = 1 - \frac{\dot{E}_{d,HPH8}}{\dot{m}_2\left(e_2 - e_{33}\right)} \quad \text{(XXXVIII)}$$

2.5. Energy and exergy simulation using the EES software

The energy and exergy analyses of the USC SPP were conducted using the EES software (Professional V10.561-3D [12.20.2018]).[22] EES was used to model the thermodynamic processes within the power plant and calculate energy and exergy flows and destruction. The thermodynamic properties of water and steam were obtained from the built-in property functions within EES. The software was selected for its capability to solve complex thermodynamic equations, perform iterative calculations, and handle multi-variable systems efficiently. The input parameters, such as mass flow rates, temperature, pressure, and specific enthalpy, were derived from the plant's operational data. A reference condition of standard pressure 1 bar or 100 kPa and temperature 25°C or 298.15 K was employed to perform the analysis. The results of the analysis were visualized using graphs and tables to highlight the efficiency trends and exergy destruction in key components, such as the boiler, turbines, and condenser.

2.6. Error analysis and assumptions

The results presented in this study are subjected to potential sources of error and are based on several simplifying assumptions. These include:

2.6.1. Operational data uncertainties

Errors may arise from uncertainties inherent in the measured operational data (e.g., pressure, temperature, mass flow rates) obtained from the plant. While specific measurement uncertainty values are proprietary and cannot be disclosed, these measurements are subjected to instrumentation accuracy and calibration limitations. To mitigate the impact of these uncertainties, we utilized data derived from comprehensive plant testing and heat balance diagrams, which represent integrated plant performance under specific operating conditions.

2.6.2. Thermodynamic modeling assumptions

Assumptions in thermodynamic modeling, such as ideal component behavior or simplified equations, can also affect the results.

2.6.3. Component simplifications

Simplifications in the representation of power plant components (e.g., neglecting minor heat losses or non-uniform flow distributions) can contribute to discrepancies between the model and the actual plant behavior.

2.6.4. Steady-state assumption

The model assumes steady-state operation, neglecting dynamic effects and transient behavior of the power plant.

2.6.5. Neglected pressure drops

Minor pressure drops in pipes are not considered in the model. This simplification may affect the accuracy of the results at specific locations within the plant.

2.6.6. Fouling effects

The model does not account for the effects of fouling on component performance. Fouling can significantly impact heat transfer rates and efficiencies over time, but the analysis does not include these effects.

While a formal uncertainty propagation analysis was not performed due to the unavailability of detailed measurement uncertainty data, the validation of the model against the plant's heat balance data, where the deviation of calculated versus real parameters was consistently below 5% (as detailed in Section 2.7), provides a level of confidence in the overall accuracy and trends identified in the exergy analysis. Future work could explore applying uncertainty quantification techniques, such as Monte Carlo simulations, if detailed measurement uncertainty data becomes accessible.

2.7. Model validation

The model's accuracy was rigorously assessed by comparing its predictions with actual operational data obtained directly from the plant's heat balance diagram. Table 4 compares key thermodynamic parameters for the XYZ USC power plant at 100% load (1,070 MW) between the simulation results and the plant's operational data. The deviation between the calculated and actual parameters for critical variables, such as boiler enthalpy, reheat steam mass flow, feedwater enthalpy, and turbine extraction mass flows was consistently below 5%.

3. Results and discussion

3.1. Energetic analysis

The efficiency of an SPP is influenced by the load applied to the power plant. The net energetic efficiency of an SPP is depicted in Figure 3, showing a comparison between actual and isentropic processes across various load percentages (50%, 75%, and 100%). The overall power plant efficiencies achieved in this study (46.94% at 50% load, 47.01% at 75% load, and 47.03% at 100% load) are comparable to those reported by Hasti *et al.*[23] for other USC power plants, which ranged from approximately 42 to 45% for the plants they analyzed. However, Braimakis *et al.*[24] reported slightly higher efficiencies (up to approximately 49%) for USC biomass-fueled plants, suggesting that fuel type and system configuration can significantly impact performance. Our study focuses on a 1,070 MW USC coal-fired plant, and variations in capacity and specific design parameters will also influence the achievable efficiency. On the other hand, the isentropic efficiency demonstrates a more pronounced increase, starting at 51.25% at 50% load and reaching 52.19% at 100% load. An isentropic process is defined as one that is both adiabatic (no heat exchange with the surroundings) and reversible (no internal entropy generation). The increase in isentropic efficiency also reflects an improvement in global isentropic efficiency, which considers the cumulative performance of multiple components, such as turbines, compressors, and pumps, rather than isolated elements. A higher global isentropic efficiency at increased loads suggests that the system as a whole operates more optimally, reducing

Table 4. Deviation simulation result

Parameter	Unit	Plant operational data	Simulation result	Deviation (%)
Boiler enthalpy	kJ/kg	3,493.7	3494	0.008
Reheat steam mass flow	kg/s	683.83	679.2	0.68
Feedwater enthalpy (to boiler)	kJ/kg	1,278.5	1,279	0.04
High-pressure heater extraction mass flow	kg/s	800.37	806.91	0.82
Intermediate-pressure heater extraction mass flow	kg/s	687.81	679.18	1.25
Low-pressure heater extraction mass flow	kg/s	556.24	545.79	1.87
Condenser mass flow	kg/s	458.33	436.1	4.85
Net power output	MW	1,070	1,035	3.27
Overall plant efficiency	%	48.61	47.03	3.25

exergy destruction and approaching ideal thermodynamic behavior. This discrepancy can be attributed to the inherent thermodynamic efficiencies of the idealized isentropic process, which does not account for real-world losses such as friction and heat dissipation. The improvement in efficiency with increasing load for both conditions is consistent with findings that higher loads typically enhance thermodynamic efficiency due to better utilization of the system's capacity and reduced relative losses.[25,26]

Additionally, Figure 4 illustrates the net plant heat rate (NPHR) for both actual and isentropic conditions at the same load percentages. The NPHR of an SPP is a crucial indicator of its efficiency, representing the amount of heat required to generate one kilowatt-hour of electricity. Analyzing the provided data for three load levels (50%, 75%, and 100%) reveals distinct patterns in efficiency. At 50% load, the actual NPHR is 3,690 kcal/kWh compared to the isentropic NPHR of 3,491 kcal/kWh. This indicates that the plant's actual performance is less efficient than the theoretical ideal by 199 kcal/kWh, or approximately 5.7%. The higher NPHR at this lower load is expected due to increased inefficiencies when the plant operates below its optimal capacity. At 75% load, the actual NPHR improves to 2,527 kcal/kWh, while the isentropic NPHR is 2,286 kcal/kWh. The gap between actual and isentropic NPHR is now 241 kcal/kWh, translating to a 10.5% difference.

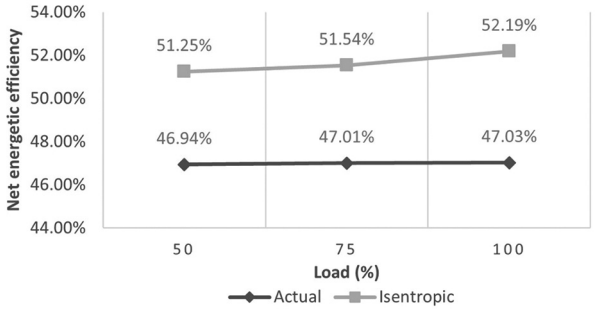

Figure 3. Comparison graph of efficiency with different loads

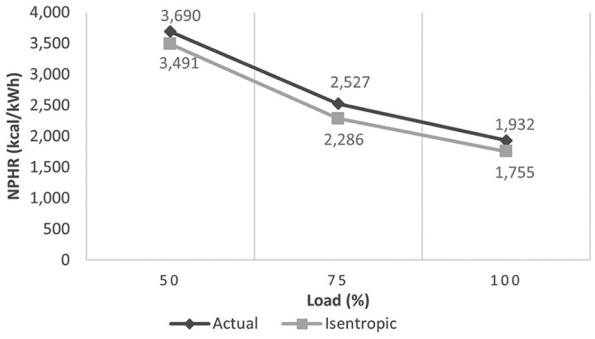

Figure 4. Comparison of net plant heat rate in actual and isentropic conditions

The reduction in NPHR from 50% to 75% load highlights the plant's improved efficiency as it operates closer to its optimal range. At full load (100%), the actual NPHR further decreases to 1,932 kcal/kWh, with the isentropic NPHR at 1,755 kcal/kWh. The difference of 177 kcal/kWh, or about 9.2%, represents the smallest gap between actual and theoretical performance across the load levels, demonstrating that the plant operates most efficiently at full capacity.

These discrepancies between actual and isentropic NPHR across different loads can be attributed to several factors, such as mechanical losses, thermodynamic inefficiencies, operational practices, and equipment conditions. Lower efficiency at partial loads is common due to suboptimal use of the plant's design capacity, leading to increased heat losses and mechanical inefficiencies. Conversely, operating near full load maximizes efficiency by minimizing these losses.

As the load increases, the NPHR decreases, demonstrating that higher loads enhance plant efficiency by optimizing energy conversion and minimizing losses.[27] This relationship underscores the importance of operating SPPs near full capacity whenever possible to achieve economic and environmental benefits.

3.2. Exergetic analysis

Exergy analysis provides detailed insight into a system's inefficiencies by quantifying the destruction of useful energy. By examining the exergy destruction and exergetic efficiency of various components under different load conditions, we can identify areas for improvement and enhance overall plant performance. Table 5 shows the exergy analysis results for a 1,070 MW USC power plant at 100%, 75%, and 50% unit loads. These results are crucial for understanding how each component contributes to the plant's overall efficiency and identifying optimization opportunities.

The data indicates significant variations in exergy destruction across the SPP's components, with the boiler consistently exhibiting the highest values. Specifically, the boiler shows exergy destruction of 1,416 MW at 100% load, 1,609 MW at 75% load, and 1,918 MW at 50% load. This high level of destruction is due to irreversibilities associated with the combustion process and heat transfer within the boiler. Several studies support this observation. One analysis highlights that the boiler is the largest source of exergy destruction in USC systems due to the high-temperature gradients and inefficiencies in fuel combustion and heat exchange processes.[23,24]

The turbines, especially the LPT, also show significant exergy destruction, with values reaching 37.31 MW at 100%

Table 5. Results of exergetic analysis

Component	Exergy destruction (MW)			Exergetic efficiency (%)		
	100%	75%	50%	100%	75%	50%
Boiler	1,416	1,609	1,918	49.56	38.73	25.41
HPT	17.25	20.81	13.40	95.25	92.56	93.13
IPT	11.09	8.11	5.40	96.84	96.92	92.12
LPT	37.31	26.09	17.29	91.14	91.99	96.89
Turbine	65.65	55.02	36.09	94.41	93.82	94.04
Condenser	5.05	4.60	3.98	88.98	85.54	82.92
CEP	1.54	1.46	1.44	37.82	37.04	25.43
LPH-1	2.80	1.70	0.54	88.98	92.64	97.25
LPH-2	3.97	2.92	0.47	89.24	90.75	97.43
LPH-3	1.60	1.31	0.84	93.81	93.87	94.31
LPH-4	3.30	2.21	1.38	93.95	94.59	94.82
Deaerator	37.93	29.23	20.11	91.75	90.76	89.36
BFP	3.08	2.44	0.89	90.48	87.4	89
HPH-6	6.34	3.68	1.87	64.04	79.85	81.51
HPH-7	5.65	3.11	2.26	87.77	91.36	90.46
HPH-8	11.39	10.48	8.61	75.21	67.39	66.56
Net				44.5	35.32	25.57

Abbreviations: BFP: Boiler feed pump; CEP: Condensate extraction pump; HPH: High-pressure heater; HPT: High-pressure turbine; IPT: Intermediate-pressure turbine; LPH: Low-pressure heater; LPT: Low-pressure turbine.

load, decreasing to 26.09 MW at 75% load, and 17.29 MW at 50% load. These losses are primarily due to friction, heat losses, and non-ideal expansion processes. Among the turbines, the HPT shows a unique trend where its efficiency initially decreases as the load decreases but then increases again. This behavior can be attributed to variations in steam inlet conditions. At lower loads, the reduction in steam pressure and temperature leads to suboptimal expansion, resulting in higher exergy destruction. However, as the load increases, steam parameters improve, allowing for a more efficient thermodynamic expansion process and contributing to the recovery of HPT efficiency. On the other hand, the IPT demonstrates an opposite pattern, where its efficiency initially increases before experiencing a decline. This fluctuation is closely linked to the reheating process. Steam reheating is more effective at moderate loads, reducing irreversibilities and improving efficiency. However, as the load decreases, the steam flow rate and temperature differentials become less favorable, increasing energy losses and leading to lower IPT efficiency. The LPT exhibits a consistent decline in efficiency across all load levels. This can be attributed to the increasing moisture content in the steam during expansion. As the steam expands, its quality deteriorates, leading to higher aerodynamic losses and blade erosion. At lower loads, reduced steam flow exacerbates these effects, further decreasing LPT efficiency.[24]

The CEP displays notably low efficiency across all operating conditions. This is primarily due to significant throttling and pressure losses within the system, which contribute to high exergy destruction. Furthermore, as a supporting component in the feedwater cycle, a significant portion of the work done by the CEP is used to overcome hydraulic resistance rather than directly contributing to power generation. These factors collectively result in the observed low-efficiency values for the CEP.

A Sankey diagram was developed to provide a visual representation of the exergy flow and destruction within the XYZ USC SPP at 100% load, as shown in Figure 5.

As depicted in the Sankey diagram (Figure 5), the total exergy input to the system at 100% load is 2,807 MW. The width of the arrows in the diagram is proportional to the magnitude of the exergy flow. The diagram clearly illustrates the exergy flow through the major components of the power plant, including the boiler, HPT, IPT, LPT, condenser, and auxiliary components such as pumps and heaters. Consistent with the quantitative results in Table 5, the Sankey diagram visually emphasizes the significant exergy destruction in the boiler (1,416 MW), represented by the widening arrow leading to "Des. Ex Boiler." Conversely, the narrow arrow indicating exergy destruction in the condenser (1.54 MW) confirms its lower contribution to overall exergy losses. The net power output of 1,035 MW is shown as the useful exergy leaving the system.

While a detailed Sankey diagram is presented for the 100% load condition, the general flow path and the components with the highest and lowest exergy destruction remain consistent across the 75% and 50% load conditions. The primary difference in the Sankey diagrams for these partial loads would be the reduced magnitudes of the exergy input, internal flows, exergy destruction in each component, and the net power output, roughly proportional to the reduction in load. The distribution of exergy destruction among the components follows a similar trend, with the boiler consistently exhibiting the largest irreversibilities.

Figure 6 shows the variation in the exergetic efficiency of all major power plant components. The analysis reveals that the boiler consistently exhibits the lowest exergetic efficiency, with a significant decline as the load decreases: 49.56% at 100% load, 38.73% at 75% load, and 25.41% at 50% load. This substantial inefficiency is attributed to high irreversibilities in the combustion process and heat transfer within the boiler, which become more

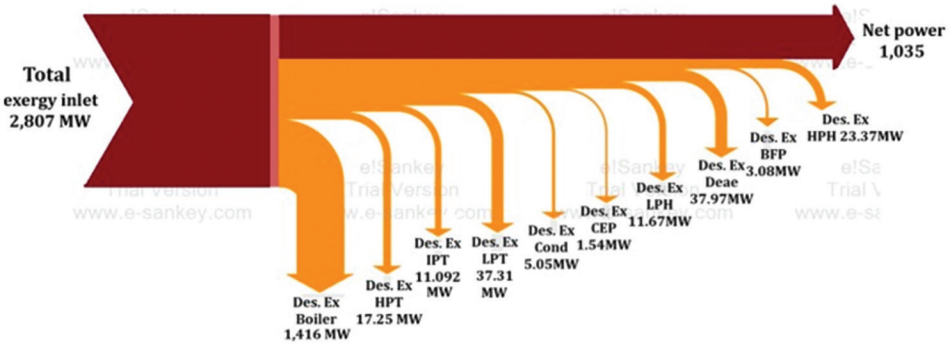

Figure 5. Exergy flow at 100% load
Abbreviation: Des.Ec: Destruction exergys.

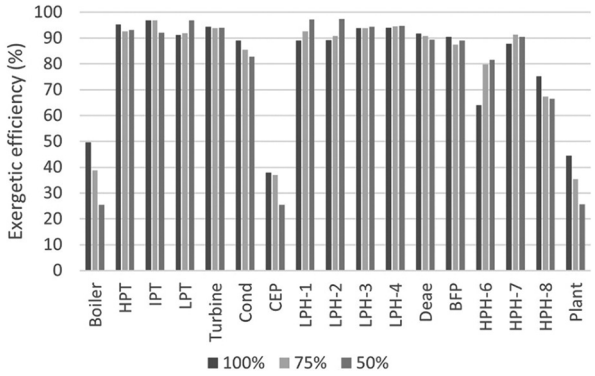

Figure 6. Exergetic efficiency of all major power plant components
Abbreviations: BFP: Boiler feed pump; CEP: Condensate extraction pump; Cond: Condenser; Deae: Deaerator; HPH: High-pressure heater; HPT: High-pressure turbine; IPT: Intermediate-pressure turbine; LPH: Low-pressure heater; LPT: Low-pressure turbine.

pronounced at lower loads. In contrast, the turbines, including the HPT, IPT, and LPT, maintain relatively high exergetic efficiencies, indicating efficient thermal to mechanical energy conversion with less variation across different loads. The condenser also shows high efficiency, with values of 88.98% at 100% load, 85.54% at 75% load, and 82.92% at 50% load due to effective heat rejection processes. LPH-1 to LPH-4 consistently demonstrates high exergetic efficiencies, efficiently recovering and utilizing waste heat. While exhibiting high efficiency, the deaerator shows a slight decrease at lower loads, indicating increased irreversibilities in removing dissolved gases from the feedwater. HPH-6 to HPH-8 have lower exergetic efficiencies than LPHs due to higher irreversibilities in the heat exchange processes at higher pressures.

Overall, this analysis underscores the need for targeted improvements in the boiler to enhance the overall exergetic efficiency of the SPP, while highlighting the relative stability and efficiency of the turbines, condenser, and heaters across varying load levels.

3.3. CO_2 emissions analysis

The potential CO_2 emissions from the XYZ USC SPP are estimated based on the assumption that the electricity generated is connected to the "Jamali" electricity system. The emission factor applicable to the "Jamali" system in 2021 was 0.87 kg CO_2 per MWh, as stipulated in the Decree of the Minister of Energy and Mineral Resources of the Republic of Indonesia[2]. This analysis estimates the monthly emissions at three different operating load conditions: 50%, 75%, and 100% of the nominal capacity.

The monthly calculations assume that the power plant operates continuously at the specified load for 720 h (representing the average number of hours in a month). At a 50% load, with an approximate power output of 541.946 MW, the estimated monthly electricity generation reaches 390,201.12 MWh. Utilizing the "Jamali" emission factor, the monthly CO_2 emissions associated with electricity production at this load are estimated to be 339,474.97 kg. When the power plant operates at a 75% load, generating approximately 791.281 MW, the monthly electricity production is estimated at 569,722.32 MWh, potentially resulting in CO_2 emissions of 495,658.42 kg/month. At full capacity (100% load) with a power output of 1,035 MW, the monthly electricity production reaches 745,200 MWh, and the estimated monthly CO_2 emissions are 648,324 kg.

These estimation results indicate that the amount of CO_2 emissions is directly proportional to the power plant's operating load. Operation at higher loads results in more electricity potentially supplied to the grid and, consequently, higher estimated CO_2 emissions. It is important to emphasize that this analysis is based on the assumptions of continuous operation at a constant load for an entire month and the use of the average emission factor for the "Jamali" system. In actual operational conditions, the power plant's load will vary, and the actual emissions may be influenced by other factors, such as the plant's efficiency at different load levels and the fuel mix

utilized within the overall grid system. Nevertheless, this estimation provides a crucial overview of the potential CO_2 emission contribution of the XYZ USC SPP within the context of its connected electricity system. While offering higher thermal efficiency compared to conventional SPP technologies, USC technology still generates CO_2 emissions due to the combustion of fossil fuels. The magnitude of these emissions is directly linked to the quantity of electricity produced and the carbon intensity of the electricity system.

4. Future work and challenges

In light of our findings, future research should focus on further optimizing the boiler design to reduce exergy destruction, exploring the integration of renewable energy sources with USC plants, and investigating the use of advanced materials to enable even higher operating temperatures and efficiencies. Challenges associated with USC technology include the high capital costs, the need for advanced materials and manufacturing techniques, and the requirement for specialized training for plant operators and maintenance personnel.

5. Conclusion

The results of the energy and exergy analyses, aligned with the research objectives, provide insights into the performance of the XYZ 1,070 MW USC coal-fired SPP. This power plant utilizes a working fluid (usually water) heated by burning coal to rotate a turbine and generate electricity. The analysis employed the first and second laws of thermodynamics to assess both energy efficiency and exergy destruction. The results indicate that the generator efficiency exhibits minimal variation across different load conditions, with values of 46.94% at 50% load, 47.01% at 75% load, and 47.03% at 100% load. The analysis also revealed significant exergy destruction within the system. The boiler consistently showed the highest exergy destruction, with values of 1,918 MW at 50% load, 1,609 MW at 75% load, and 1,416 MW at 100% load. This highlights the boiler as a key area for potential improvement in overall plant efficiency. In contrast, the CEP exhibited the lowest exergy destruction, with values of 1.441 MW at 50% load, 1.457 MW at 75% load, and 1.544 MW at 100% load.

Considering the environmental implications of coal-fired power generation, a simplified estimation of potential CO_2 emissions was conducted, assuming a connection to the "Jamali" electricity system (emission factor: 0.87 kg CO_2/MWh). While not the core focus of this study, the estimates indicate a load-dependent trend in emissions: 339,474.97 kg/month at 50% load, 495,658.42 kg/month at 75% load, and 648,324 kg/month at 100% load. Based on continuous operation assumptions, these values highlight the substantial CO_2 output associated with the plant's operation.

Acknowledgments

The authors express sincere gratitude to all individuals and institutions that have provided invaluable support during the research and preparation of this manuscript. Special thanks to the faculty members and administrative staff of the Department of Mechanical Engineering, Diponegoro University, whose guidance and assistance have been instrumental in completing this study. The authors also deeply appreciate the insightful feedback and encouragement provided by colleagues and peers, which greatly enhanced the quality of the research.

The authors extend profound thanks to the XYZ SPP for granting access to its facilities, data, and specialized equipment, which played a crucial role in the completion of this study. This support has been invaluable in ensuring the accuracy and relevance of the research findings. Finally, heartfelt thanks are conveyed to family and friends for their unwavering moral support throughout the research process.

Funding

None.

Conflict of interest

The author declares that they have no competing interests.

Author contributions

Conceptualization: Fadhlin Nurul Izzah, Berkah Fajar Tamtomo Kiono
Formal analysis: Fadhlin Nurul Izzah
Investigation: Berkah Fajar Tamtomo Kiono
Methodology: All authors
Writing – original draft: Fadhlin Nurul Izzah
Writing – review & editing: Khoiri Rozi, Berkah Fajar Tamtomo Kiono

Ethics approval and consent to participate

Not applicable.

Consent for publication

Not applicable.

Availability of data

The data used in this study consists of quantitative data derived from both primary and secondary sources. This

data are not publicly available and can be accessed with permission from the relevant authorities at XYZ SPP.

Further disclosure

The entire set of findings from this study was presented at the SET2024 (21st International Conference on Sustainable Energy Technologies), Shanghai, China, on August 12 – 14, 2024.

References

1. Nepal R, Paija N. Energy security, electricity, population and economic growth: The case of a developing South Asian resource-rich economy. *Energy Policy*. 2019;132:771-781.

   doi: 10.1016/j.enpol.2019.05.054

2. Kementrian Energi dan Sumber Daya Mineral Republik Indonesia. *Keputusan Menteri Energi dan Sumber Daya Mineral Republik Indonesia Nomor 188.K/HK.02/MEM. L2021tentang Pengesahan Rencana Usaha Penyediaan Tenaga Listrik PT Perisahaan Listrik Negara (Persero)* [*Decree of the Minister of Energy and Mineral Resources of the Republic of Indonesia Number 188.K/HK.02/MEM.L/2021 on the Approval of the Electricity Supply Business Plan of PT Perusahaan Listrik Negara (Persero)]*. Indonesia: Kementrian ESDM; 2021.

3. Fan H, Zhang Z, Dong J, Xu W. China's R and D of advanced ultra-supercritical coal-fired power generation for addressing climate change. *Thermal Sci Eng Prog*. 2018;5:364-371.

   doi: 10.1016/j.tsep.2018.01.007

4. Eguchi S, Takayabu H, Lin C. Sources of inefficient power generation by coal-fired thermal power plants in China: A metafrontier DEA decomposition approach. *Renew Sustain Energy Rev*. 2021;138:110562.

   doi: 10.1016/j.rser.2020.110562

5. Zhang C, Wang Z. Comprehensive energy efficiency analysis of ultra-supercritical thermal power units. *Appl Therm Eng*. 2023;235:121365.

   doi: 10.1016/j.applthermaleng.2023.121365

6. Nikam KC, Kumar R, Jilte R. Exergy and exergo-environmental analysis of a 660 MW supercritical coal-fired power plant. *J Therm Anal Calorim*. 2021;145(3):1005-1018.

   doi: 10.1007/s10973-020-10268-y

7. Rocha DHD, Siqueira DS, Silva RJ. Effects of coal compositions on the environment and economic feasibility of coal generation technologies. *Sustain Energy Technol Assess*. 2021;47:101500.

   doi: 10.1016/j.seta.2021.101500

8. Cengel YA, Boles MA. *Thermodynamics: An Engineering Approach. Introduction and Basic Concepts*. 8th ed., Ch. 1. United States: McGraw-Hill Education; 2015.

9. Ersayin E, Ozgener L. Performance analysis of combined cycle power plants: A case study. *Renew Sustain Energy Rev*. 2015;43:832-842.

   doi: 10.1016/j.rser.2014.11.082

10. Han T, Wang C, Zhu C, Che D. Optimization of waste heat recovery power generation system for cement plant by combining pinch and exergy analysis methods. *Appl Therm Eng*. 2018;140:334-340.

    doi: 10.1016/j.applthermaleng.2018.05.039

11. Chen H, Wang Y, Yan L, Wang Z, He B, Fang B. Energy and exergy analysis on a blast furnace gas-driven cascade power cycle. *Energies (Basel)*. 2022;15(21):8078.

    doi: 10.3390/en15218078

12. Khaleel OJ, Basim Ismail F, Khalil Ibrahim T, Bin Abu Hassan SH. Energy and exergy analysis of the steam power plants: A comprehensive review on the classification, development, improvements, and configurations. *Ain Shams Eng J*. 2022;13(3):101640.

    doi: 10.1016/j.asej.2021.11.009

13. Adibhatla S, Kaushik SC. Energy and exergy analysis of a super critical thermal power plant at various load conditions under constant and pure sliding pressure operation. *Appl Therm Eng*. 2014;73(1):51-65.

    doi: 10.1016/j.applthermaleng.2014.07.030

14. Pambudi NA, Itoi R, Jalilinasrabady S, Jaelani K. Exergy analysis and optimization of Dieng single-Flash geothermal power plant. *Energy Convers Manag*. 2014;78:405-411.

    doi: 10.1016/j.enconman.2013.10.073

15. Kaushik SC, Reddy VS, Tyagi SK. Energy and exergy analyses of thermal power plants: A review. *Renew Sustain Energy Rev*. 2011;15(4):1857-1872.

    doi: 10.1016/j.rser.2010.12.007

16. Kumar V, Saxena VK, Kumar R, Kumar S. Energy, exergy, sustainability and environmental emission analysis of coal-fired thermal power plant. *Ain Shams Eng J*. 2024;15(2):102416.

    doi: 10.1016/j.asej.2023.102416

17. Abuelnuor AAA, Hassan Suliman MM, Abuelnour MA, Younis O, Mohamed EF. Exergy analysis of the boiler in phase 3 of the Khartoum North power plant. *Results Eng*. 2024;21:101919.

    doi: 10.1016/j.rineng.2024.101919

18. Khaleel OJ, Ibrahim TK, Ismail FB, Al-Sammarraie AT, Hassan SHBA. Modeling and analysis of optimal performance of a coal-fired power plant based on exergy evaluation. *Energy Rep*. 2022;8:2179-2199.

    doi: 10.1016/j.egyr.2022.01.072

19. Mohamed O, Khalil A, Wang J. Modeling and control of supercritical and ultra-supercritical power plants: A review.

Energies (Basel). 2020;13(11):2935.

doi: 10.3390/en13112935

20. Qasem M, Mohamed O, Elhaija WA. Parameter identification and sliding pressure control of a supercritical power plant using whale optimizer. *Sustainability (Switzerland)*. 2022;14(13):8039.

doi: 10.3390/su14138039

21. Abe F. Research and development of heat-resistant materials for advanced USC power plants with steam temperatures of 700 °C and above. *Engineering*. 2015;1(2):211-224.

doi: 10.15302/J-ENG-2015031

22. Klein SA. *Engineering Equation Solver*. Madison: University of Wisconsin; 2018.

23. Hasti S, Aroonwilas A, Veawab A. Exergy analysis of ultra super-critical power plant. In: *Energy Procedia*. Vol. 37. Netherlands: Elsevier Ltd.; 2013. p. 2544-2551.

doi: 10.1016/j.egypro.2013.06.137

24. Braimakis K, Magiri-Skouloudi D, Grimekis D, Karellas S. Energy-exergy analysis of ultra-supercritical biomass-fuelled steam power plants for industrial CHP, district heating and cooling. *Renew Energy. 2*020;154:252-269.

doi: 10.1016/j.renene.2020.02.091

25. Chen C, Bollas GM. Dynamic optimization of a subcritical steam power plant under time-varying power load. *Processes*. 2018;6(8):114.

doi: 10.3390/pr6080114

26. Karakurt AS, Güneş Ü. *Performance Analysis of a Steam Turbine Power Plant at Part Load Conditions*. Vol. 3. Turkey: Yildiz Technical University Press; 2017.

27. Napitu PYG, Setiyana B. Net plant heat rate (NPHR) analysis of main plant boiler unit (UIK) towards coal additive corint PC 99 injection. *Int Res J Innovat Eng Technol (IRJIET)*. 2022;6(8):31-35.

doi: 10.47001/IRJIET/2022.608005